Efficient Excitation of Characteristic Modes for Radiation Pattern Control by Using a Novel Balanced Inductive Coupling Element

Francesco Alessio Dicandia, *Student Member, IEEE,* Simone Genovesi, *Member, IEEE*, and Agostino Monorchio, *Fellow, IEEE*

Equation Chapter 1 Section 1

***Abstract*—A design strategy exploiting the Characteristic Modes Analysis (CMA) is described for improving the radiation efficiency of a mounted-on-platform radiator. To this aim, a novel Balanced Inductive Exciter (BIE) is introduced to improve the modal excitation purity of some Characteristic Modes (CMs). In fact, even if the optimal position of the exciters on the hosting platform is determined by using the Characteristic Modes Theory (CMT), the excitation purity of each mode plays a fundamental role in the radiation efficiency of the radiating system. In particular, achieving a good level of excitation purity strongly reduces the reactive power (P_{reac}) stored in the near field zone and hence maximizes the amount of the radiated power (P_r). To better highlight the benefits offered by the presented approach, a set of BIEs is applied on a platform to obtain a fully-reconfigurable radiation pattern. The evaluation of the P_{reac}, P_r and Equivalent Isotropically Radiated Power (EIRP) provided by the BIE reveals the importance of a pure modal excitation. To assess the reliability of the proposed BIEs some prototypes have been manufactured and tested.**

***Index Terms*—Characteristic modes, radiation pattern control, beam-steering, pattern reconfigurable antenna, inductive excitation.**

I. Introduction

The design of an antenna is as much challenging as the hosting object is a platform that imposes constraints on the form factor of the antenna, limits the overall available space and requires the radiating element to be close to a metallic surface. This can be the case of a vehicle, a ship or a drone that may require small and conformal antennas. This is a challenging task, especially in the sub-GHz frequency region, which can be faced by using convoluted elements or adding distributed loads [1], [2]. Moreover, the placement of an antenna on a complex metallic platform (*e.g.* vehicles, aircraft, ship) deeply affects its radiating performance. A promising strategy to cope with these problems consist of making an antenna able to exploit the platform.

Indeed, this idea is not completely new since the first attempts dates back to the 50's when the metallic structure of an aircraft was used as a radiating element in [3]–[4]. More recently, a side-mounted configuration of Very High Frequency (VHF) half loop antennas for an helicopter platform was proposed in [5] to exploit the platform as main radiator and reduce the rotor modulation. Other solutions that employ half loops as a coupler to induce on the metallic object a desirable current distribution are reported in [6], [7].

Moreover, a Naval Structural Antenna (NSA), which is able to use the hosting metallic structure as radiator, has been introduced in [8]–[10] for High-Frequency (HF) shipboard antenna. However, the aforementioned solutions [3]–[4] set a priori the location of the radiator and its kind (dipole, slot) and are often resonant elements. Additionally, the NSA [8]–[10] concept excited the currents only on a portion of the investigated object.

On the contrary, the Characteristic Modes Theory (CMT) [11] that has recently been applied in the field of antenna design, provides a detailed picture of all the potentialities offered by the hosting platform regardless of any a priori choice of exciters and feeding arrangement. The benefits of the CMT have been demonstrated in [12]–[16] where different MIMO antenna systems are designed by exploiting the Characteristic Modes (CMs) of different rectangular boards. A null-steering antenna obtained by exploiting an asymmetrical excitation of two CMs was described in [17] whereas a three dimensional null-scanning antenna based on the selective excitation degree of the current modes (J_n) over hosting device has been proposed in [18]. The advantageous exploitation of the CMs analysis have been also verified in [19]–[21] for massive MIMO application, phased array and wideband metasurface antenna.

In addition to the aforementioned applications, the CMT has been recently applied for three dimensional platform [22]–[25], as well. More in detail, in [22], [23] the CMT are exploited to identify the optimum positions for some exciters on an Unmanned Aerial Vehicle (UAV) and to obtain a desirable radiating current on a ship, respectively. A tunable four-ports MIMO antenna system for cognitive radio (CR) able to excite the most efficient capacitive CMs on a femto-cell device is presented in [24]. In [25], the enhancement of the bandwidth of a platform-mounted HF loop antenna system has been successfully pursued by resorting to strategically-located half loop exciters able to stimulate the suitable CMs.

The authors are with Dipartimento di Ingegneria dell'Informazione, University of Pisa, Pisa 56122, Italy (www.dii.unipi.it) and also with the CNIT, Parma 43124, Italy (www.cnit.it).

(e-mail: alessio.dicandia@for.unipi.it, simone.genovesi@unipi.it, agostino.monorchio@unipi.it).

As already mentioned, by resorting to the CMT the platform acts as the main radiative element whereas the exciters behaves like couplers to stimulate on the platform itself the desired CMs. An overview about the capacitive and inductive exciters for small terminals is presented in [26] while, a small half loop hosted above the three dimensional platform as Inductive Coupling Exciter (ICE), is introduced in [25]. Although many studies have shown a benefit from the knowledge of the best locations for placing the exciters, few efforts have been done toward the importance of modal excitation purity.

The main goal of this paper is to highlight that, even if the optimal positions of the exciters are determined from the CMT [26], [27], the modal excitation purity of the employed exciters plays an important role in the radiation efficiency of the overall radiating system. More in detail, a better excitation purity of the desired selected modes can be advantageously exploited in case of multiple CMs excitation on the investigated platform [28], which are necessary to achieve a radiation pattern control by means of the phase-shifted CMs approach [17], [18].

To improve the modal excitation purity of some CMs over the rectangular box, a novel Balanced Inductive Exciter (BIE) composed of two symmetric half loops is proposed. Moreover, a beam-steering capability is achieved by tuning the excitation degree of the multiple CMs over the rectangular box thanks to a proper amplitude and phase manipulation of the BIEs.

To underline the usefulness of a better excitation purity of the single modes, the performance in term of reactive power (P_{reac}), radiated power (P_r) and the Equivalent Isotropically Radiated Power (EIRP) attained by means of the novel BIEs, has been also compared with the previous ICEs composed of a single half loop [5]–[7], [25]. The results showed that the better excitation purity of the single modes by means of the novel BIEs strongly reduces the reactive power (P_{reac}) stored in the near field zone, and also significantly improves the radiated power (P_r) of the system in far field region. Unlike [25], the improvement of the power balance of the system is not due to the increase of the exciters number but to a better modal excitation purity of each employed exciter.

This paper is organized as follows. In Section II, the CMs analysis of a rectangular box and the optimal position for inductive exciters to efficiently stimulate the most efficient CMs is addressed. The novel BIE and its modal excitation purity is presented in Section III. Section IV is devoted to the pattern control capability by resorting to the phase-shifted CMs. Performance comparison with respect to the previous ICSs are also attained with a statistical point of view. Finally, the conclusions are reported in Section V.

II. CMs Analysis of a Three-Dimensional Platform

According to the CMT, the total current distribution (J_{tot}) on a complex object can be decomposed in terms of linear superposition of orthogonal current modes (J_n) [29]. The visualization of these orthogonal current modes (J_n) can be usefully exploited in the design process of exciters mounted on that object. In fact, depending on the position and the kind of the external exciters, it is possible to stimulate current modes (J_n) on the hosting platform, which contributes to meet the desired requirements. Moreover, to achieve an efficient radiation and thus minimizing the reactive power of the system, current modes (J_n) with the largest Modal Significance (MS) within the frequency range of operation [22] have to be excited.

The investigated three-dimensional platform with its geometrical dimensions is illustrated in Fig. 1. The dimensions are comparable to those of a vehicle and the band of interest for the analysis is within the VHF band.

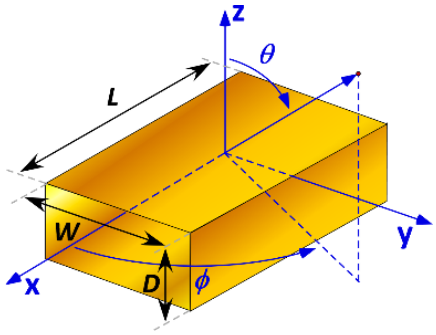

Fig. 1. Rectangular box: L = 3.4 m, W = 2 m, D = 1 m.

The CMs of the rectangular box have been calculated by using the commercial full-wave software FEKO [30] and the MS of the first five modes within the 50 MHz-80 MHz bandwidth are reported in Fig. 2 as a function of the frequency. In this study, our attention has been focused within 60 MHz-70 MHz, where the first five modes exhibit a large modal significance. This parameter is very important since it highlights which modes are in resonance (MS = 1), or near to the resonance, and therefore gives a large contribution to the total radiated power (P_r) in a particular frequency range of operation. Only the first five modes are reported in Fig. 2 because the other ones are characterized by a small value of the MS and hence they can be neglected. The current modes distribution related to the first five modes are shown in Fig. 3. It can be observed that each mode presents maxima and minima of the current in different positions and with different current orientations on the rectangular box.

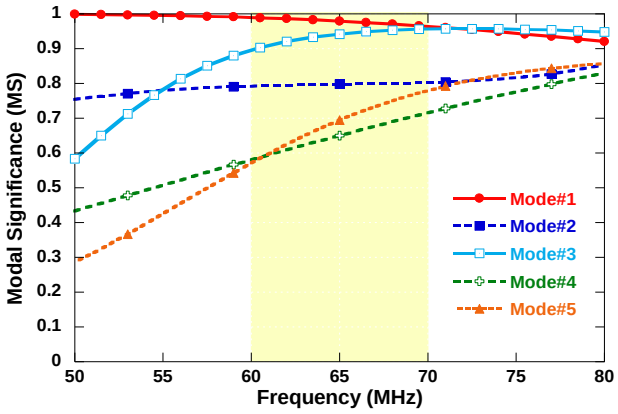

Fig. 2. Modal significance (MS) of the first five characteristic modes (J_n) as a function of the frequency.

More in detail, Mode#1 has a current distribution polarized only along x axis and it can be seen as a dipole mode along x axis. Mode#2 presents the same behavior of Mode#1, but

rotated of 90°. Mode#3 and Mode#4 are characterized by a more complicated current distribution with both the *x* and *y* components and finally Mode#5 is characterized by two out-of-phase flows of current along *x*.

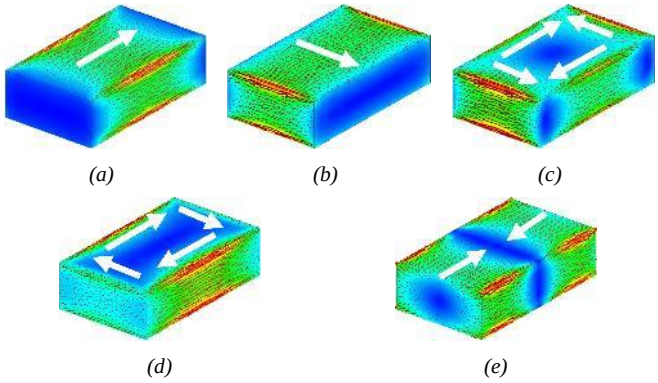

Fig. 3. Current modes distribution over the box of the first five characteristic modes (J_n); *(a)* Mode#1, *(b)* Mode#2, *(c)* Mode#3, *(d)* Mode#4, *(e)* Mode#5.

Fig. 4 displays the normalized radiation patterns of the first five CMs. As it is evident, the first two modes present a radiation pattern very similar to a dipole along *x* and *y* axis respectively. Conversely, the other three modes (Mode#3, Mode#4 and Mode#5), are characterized by a complex radiation pattern due to a different current orientation of the current modes distribution (J_n) on the investigated box as apparent in Fig. 3*c-d-e*.

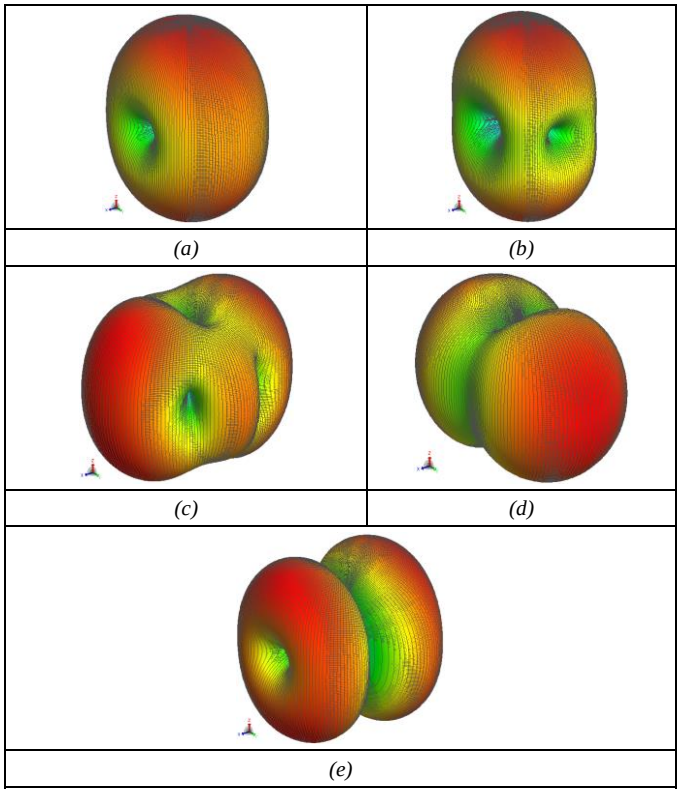

Fig. 4. Normalized modes radiation pattern related to *(a)* Mode#1, *(b)* Mode#2, *(c)* Mode#3, *(d)* Mode#4 and *(e)* Mode#5.

Once these modals radiation pattern are known, the total radiated field can be accurately represented as a weighted combination of these radiated fields, as shown in Fig. 4. Obviously, the contribution of a mode depends on the adopted feeding strategy.

A. Multiple CMs Excitation

To excite multiple CMs over the platform for achieving a radiation pattern control [18], a set of non-resonant elements should be properly collocated along the platform. In order to provide a design with the minimum impact on the carrier, any cut in the platform is avoided and the exciters can be placed only along the top side. To efficiently stimulate a particular CM over the platform, an appropriate position, amplitude and phase control is required for each exciters [26]. By analyzing the current distribution of the modes (J_n) over the platform, it is apparent that the simplest way to excite multiple CMs consists of applying four ICEs in the middle of each side of the top rectangular face, as illustrated in Fig. 5. In fact, to enhance the coupling between the desired mode and ICEs, the sources should be placed at the maximum of the current distribution of the desired modes [26]. The first four modes present a maximum of the current in the middle of each side of the top rectangular face with a different current orientation. Only Mode#5 presents a null of the current in the middle of the longest sides and hence it will not be stimulated by the ICEs. Furthermore, to maximize the excitation degree with a desired mode, the equivalent magnetic current generated by the ICEs should be parallel to the magnetic field of the mode itself. For this reason, an appropriate phase difference between the ICEs has to be guaranteed.

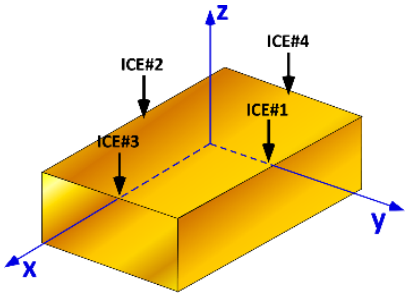

Fig. 5. Position of the ICEs over the rectangular box to efficiently stimulate the first four CMs.

By considering the CMT, the total current distribution (J_{tot}) over the investigated platform can be decomposed as [29]:

$$J_{tot} = \sum_n \alpha_n J_n \qquad (1)$$

where α_n represents the Modal Weighing Coefficient (MWC) [17] of the n^{th} CM and J_n its current modes distribution. However, by employing a set of external exciters over the box the linear superposition of equation (1) can be applied for each exciter. Therefore, by taking into account the external inductive exciters, as well as the CMs decomposition (1), the total current distribution (J_{tot}) over the investigated platform can be written as:

$$J_{tot} = \sum_n \left(\sum_k X_k \alpha_n^{(k)} \right) J_n \ , \ k = 1, \ldots, K \qquad (2)$$

where K represents the total number of the employed exciters,

X_k the feeding related to the k^{th} exciter and $\alpha_n^{(k)}$ the coupling degree between the k^{th} source and n^{th} current mode (J_n), namely the MWC of the k^{th} exciter. Unlike the current modes (J_n) distribution, the MWC values are deeply influenced by the employed exciters and the related feeding arrangement. Therefore, an appropriate choice of the exciters, as well as the related feeding arrangement, enable to achieve a selective excitation of the modes or a weighting combination of them [18]. In other words, it is possible to implement a modal filtering by means of the external sources.

By placing the ICEs in the positions illustrated in Fig. 5, it is possible to independently excite the first four modes. More in detail, to stimulate Mode#1 or Mode#2, only two ICEs along the longest (Port 1-2) or shortest (Port 3-4) side are required, respectively. Moreover, each couple has to be fed in phase since the current modes distribution presents the same orientation along *x* and *y* axis, respectively. Regarding the other two modes, namely Mode#3 and Mode#4, all the four ICEs are necessary. In addition, in this case, the orientation of the current modes distribution, allows achieving the required phase to stimulate the desired mode. The optimal feedings are summarized in Table I.

In the next section, a novel Balanced Inductive Exciter (BIE) comprising two symmetric half loops will be introduced and compared with an ICE composed of only a single half loop to prove the better modal excitation purity of the former.

TABLE I
FEEDING SETTING TO INDIVIDUALLY STIMULATE EACH MODE

Port	Amplitude (Phase)			
	Mode#1	Mode#2	Mode#3	Mode#4
#1	1(0°)	0	1(0°)	1(0°)
#2	1(0°)	0	1(180°)	1(180°)
#3	0	1(0°)	1(0°)	1(180°)
#4	0	1(0°)	1(180°)	1(0°)

III. BALANCED INDUCTIVE EXCITERS (BIES)

A new kind of exciter is proposed to stimulate the proper current distribution on the platform and the difference with respect to a commonly adopted solution is investigated. In particular, the modal excitation purity of each single mode provided by the proposed inductive exciter will be compared with the one offered by the ICE based on a small loop with one side short-circuited to the conductive plane of the platform and the feeding located to the other side of the loop. Conversely, the novel proposed ICE is implemented by using two small half loops with the outer side short-circuited to the conductive plane of the platform and the feeding points located to the inner side. Additionally, to guarantee the same flow of the current along the loops, and hence two in-phase equivalent magnetic currents (M), the two feedings are fed out-of-phase (Fig. 6*c*). The old configuration can be seen as an Unbalanced Inductive Exciter (UIE) whereas, the new one, is called Balanced Inductive Exciters (BIE). In Fig. 6*a*-*b*, the rectangular box with ICEs located on the top face, is reported for both the UIEs and BIEs configuration.

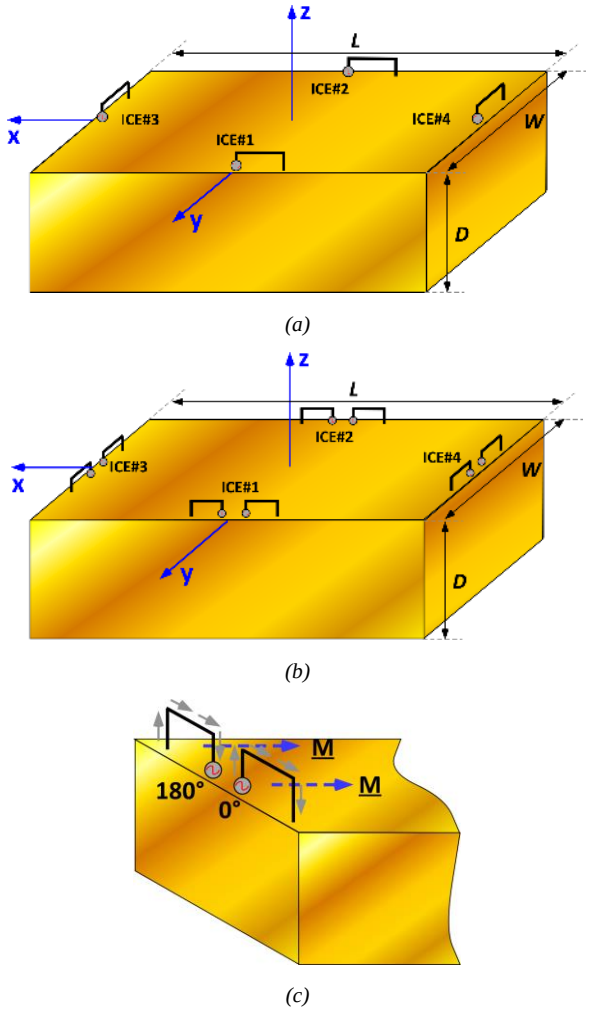

Fig. 6. ICEs arrangement over the rectangular box; *(a)* unbalanced inductive exciter (UIE), *(b)* the novel balanced inductive exciter (BIEs) configuration and *(c)* two equivalent magnetic current of the BIE.

To understand which modes are stimulated by means of the four ICEs hosted in the middle of each side of the top rectangular plate, the normalized MWC amplitude of each mode has been evaluated when the exciters are individually stimulated (Fig. 7). These values represent the $\alpha_n^{(k)}$ coefficient reported in the equation (2). In particular, both the UIEs and BIEs feeding arrangement have been compared when Port 1 and Port 2 are stimulated (Fig. 7*a*) and when Port 3 and Port 4 are on (Fig. 7*b*).

The normalized MWC reveals that the BIEs arrangement enables to stimulate over the platform only the first four modes. In particular, all the BIEs allow exciting both Mode#3 and Mode#4, whereas the couple of BIEs along *y* axis are able to stimulate also Mode#1 (Fig. 7*a*) while Mode#2 is stimulated by the BIEs along *x* axis (Fig. 7*b*). On the contrary, in the case of UIE, all the ports stimulate all the first five modes, although more or less effectively.

From this preliminary analysis, it is evident that the excitation arrangement of the novel BIEs allows achieving a better modal selective excitation than the unbalanced feed configuration (UIEs).

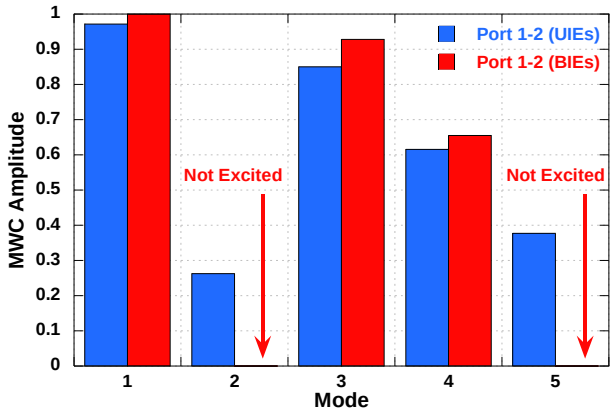

(a)

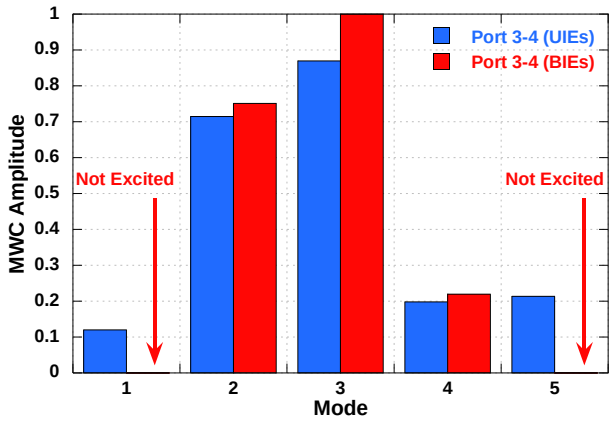

(b)

Fig. 7. Comparison of the normalized MWC amplitude between the UIEs and BIEs configuration over the box when are individually stimulated; *(a)* ports 1-2 and *(b)* ports 3-4.

Therefore, it is possible to reach a better excitation purity of the first four modes by a proper amplitude and phase manipulation of each inductive source as previously reported in Table I.

Furthermore, it is worth noting that any alteration of the investigated object affects the CMA by altering the eigenvalues behaviors with respect to the frequency and the current distribution of the modes over the object. However, since the introduced inductive exciters are electrically small, the CMA performed initially on the rectangular box can be considered valid [18].

It is important to underline that, both BIEs and UIEs, are electrically small and thus do not contribute to the radiated fields, although they differ in their ability to efficiently excite CMs on the platform.

To assess the selectivity in mode excitation of the BIEs, the percentage power excitation has been analyzed [31]. By exploiting the orthogonality of modes and the equation (2), the percentage power excitation of each mode (P_n^{rad}) is evaluated as:

$$P_n^{rad} = \left| \sum_k X_k \alpha_n^{(k)} \right|^2 \qquad (3)$$

The normalized percentage power excitation evaluated by using the amplitudes and phase differences reported in Table I and the MWC of each exciter ($\alpha_n^{(k)}$), is shown in Fig. 8.

Looking at Fig. 8 it is possible to verify that the first four modes can be independently excited by means of the feeding arrangement reported in Table I. More in detail, Mode#1, Mode#2 and Mode#3 present a very high modal excitation purity. On the contrary, Mode#4, is characterized by a slightly

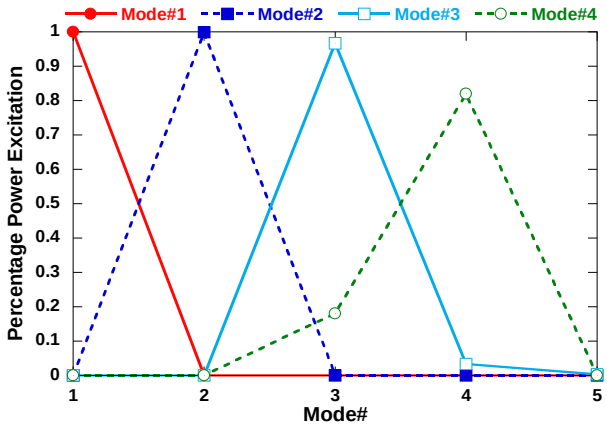

(b)

Fig. 8. Normalized percentage power excitation by using the BIEs and the appropriate feeding requirement to individually excite the first four modes evaluated at 65 MHz.

lower excitation purity due to the weak excitation of the Mode#3.

Fig. 9 shows the surface current distribution over the platform evaluated at 65 MHz when each mode is individually excited.

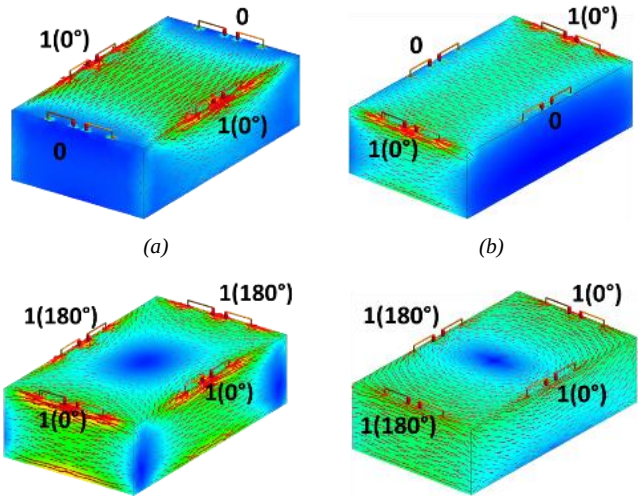

(a) *(b)* *(c)* *(d)*

Fig. 9. Simulated surface current distribution over the box by employing the BIEs as a function of external feeding. *(a)* Mode#1, *(b)* Mode#2, *(c)* Mode#3 and *(d)* Mode#4.

As it can be seen, the first three total current distributions (Fig. 9*a-b-c*) resemble very well to the related current modes distribution (J_n) previously shown in Fig. 3. Conversely, the

total surface current distribution of Mode#4 (Fig. 9*d*) does not present a very good agreement with respect to the ideal Mode#4 current distribution (Fig. 3*d*), as expected from the previous analysis (Fig. 8).

The comparison in terms of the normalized percentage power excitation of each mode by using the BIEs and the UIEs feeding arrangement has been performed in order to assess the modal excitation purity of each single mode achievable with the two different exciters. The feeding configurations are those illustrated in Table I and the results of this comparison are summarized in Table II. It is apparent that the BIEs outperform the UIEs in terms of modal excitation purity of each mode. In particular, the BIEs are capable to provide a mean improvement of the power excitation between 9.89% to 12.3% regarding Mode#1, Mode#2 and Mode#4. On the contrary, the excitation of Mode#3, presents a comparable excitation purity, even if, the BIEs enhance the purity of 2.1%. It is worth noting that Mode#4, independently of the employed exciters, does not present a modal excitation purity as high as the other three modes since it is characterized by a lower MS than that exhibited by the first three modes (Fig. 2).

TABLE II
NORMALIZED POWER EXCITATION OF THE SINGLE MODES AS A FUNCTION OF THE EMPLOYED INDUCTIVE EXCITERS

Exciters	Power Excitation			
	Mode#1	Mode#2	Mode#3	Mode#4
BIEs	1	1	0.96	0.82
UIEs	0.89	0.91	0.94	0.74
Improvement	12.3%	9.89%	2.1%	10.8%

IV. RADIATION PATTERN CONTROL CAPABILITY

Up to now, it has been proved that by exploiting the BIEs it is possible obtain a better modal excitation purity of the single current modes (J_n) over the platform. However, more than one mode has to be stimulated simultaneously with a proper weight to obtain a complete pattern control. More in detail, a beam- steering capability is achieved by tuning the excitation degree of the multiple CMs by adopting a proper amplitude and phase manipulation of the BIEs. The feeding arrangement of the BIEs that is necessary to maximize the directivity (D) in a desired direction (θ, ϕ) is retrieved by means of a genetic algorithm (GA) optimization performed in MATLAB [32]. The beam-steering capability has been also designed with the UIEs to highlight the benefits of the better modal excitation purity guaranteed by the BIEs. A comparison of the obtained results has been carried out in terms of D, percentage power excitation, P_{reac}, P_r and EIRP.

A. Directivity and Modal Power Excitation

The maximum directivity (D) as a function of the main beam direction is shown in Fig. 10*a*-*b* for both the BIEs and UIEs exciters. The color maps highlights that both the exciters are able to obtain a comparable maximum directivity in all directions with small differences. Indeed, the Cumulative Distribution Function (C.d.F) of the directivity presents very similar statistical behaviors (Fig. 10*c*) for both the ICEs.

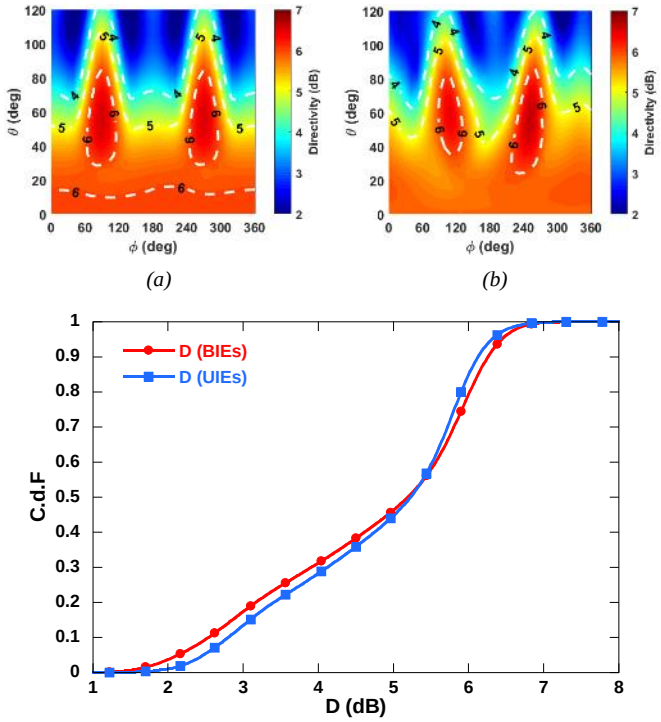

Fig. 10. Maximum directivity (D) as a function of the main beam direction by employing the *(a)* BIEs and *(b)* the UIEs. *(c)* C.d.F comparison of the D by using both the BIEs and UIEs exciters.

The reason for which the two ICEs present a comparable maximum directivity in all directions can be explained by the required percentage power excitation necessary to provide the maximum D in a desired direction. The percentage power excitation as a function of the main beam direction is reported in Fig. 11. The color maps of the same Fig. 11 show that both the ICEs provide a similar modal power excitation of the first four modes in almost all directions. In particular, Mode#2 represents the most excited current mode when the main beam direction is nearby of broadside direction ($\theta = 0°$). However, Mode#2 intensity fades little by little with the increasing of θ angle, whereas Mode#3 and Mode#4 gradually become stronger and stronger. Mode#3 gives a significant contribution to the total radiated power when the required main beam direction exceeds $\theta = 20°$ and the ϕ angles are near to the $\phi = 0°$ and $\phi = 180°$. Conversely, Mode#4 presents the same behavior, but for different ϕ angles and with a slightly lower maximum power excitation. Moreover, it is possible to observe that thanks to the symmetry of the BIEs, the related modal power excitation of all modes are perfectly symmetric with respect $\phi = 180°$. On the contrary, by resorting to the UIEs the modal power excitation symmetry is not present. Obviously, there are some zones in which the modal power excitation are somewhat different, especially in the directions where the UIEs excites also Mode#5, since the BIEs does not stimulate this mode. This is the reason that generates some discrepancy in the maximum D visible in the color maps of Fig. 10*a*-*b* and in their statistical behavior shown in Fig. 10*c*.

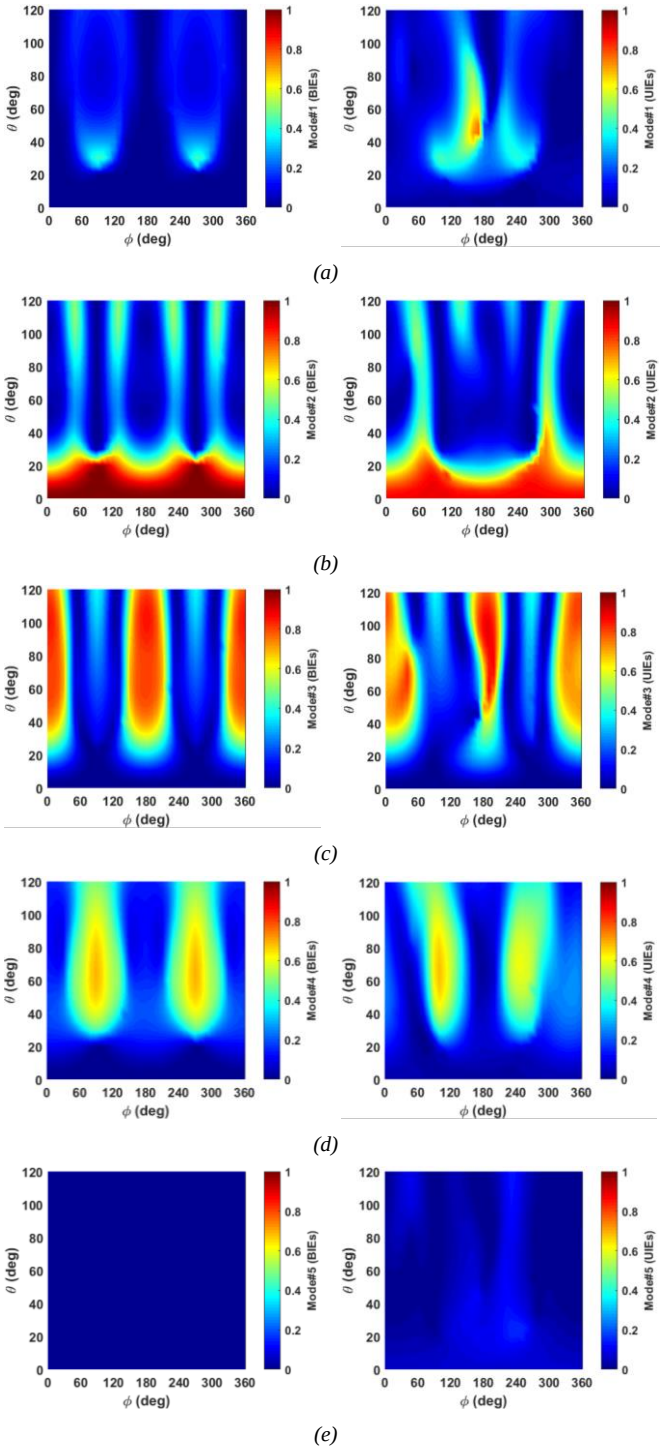

Fig. 11. Percentage power excitation as a function of the main beam direction necessary to provide the maximum *D* for Mode#1 *(a)*, Mode#2 *(b)*, Mode#3 *(c)*, Mode#4 *(d)* and Mode#5 *(e)*. Left column refers to BIEs whereas right one to UIEs.

In order to better underline the similarity of the modal power excitation, the mean value of the power excitation of the five modes, necessary to realize the beam-steering capability, is illustrated in Fig. 12. As it is evident, the two ICEs shows a comparable mean value of the modal power excitation, as previously stated. In particular, Mode#2, Mode#3 and Mode#4 undergo a slightly higher mean power excitation by resorting to the BIEs, whereas Mode#1 is somewhat better stimulated in case of UIEs. Moreover, in case of the UIEs the total radiated power has the contribution of Mode#5 as previously shown through the Fig. 7 and Fig. 11*e*.

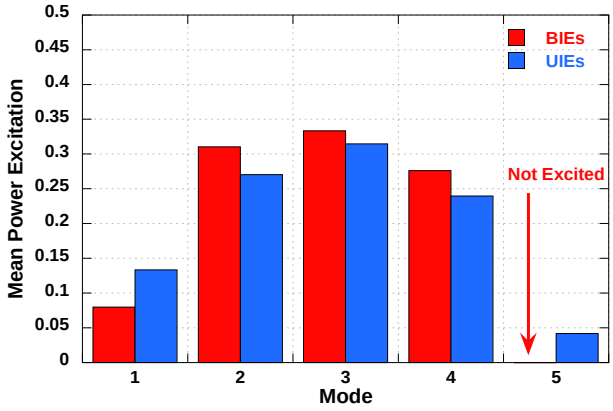

Fig. 12. Mean modal power excitation of the first five modes by using both the BIEs and the UIEs.

Therefore, the BIEs do not improve the maximum directivity of the radiating system with respect to the UIEs when the beam-steering capability is implemented.

B. Power Balance Improvement by Means of BIEs

With the purpose of understanding if a better modal excitation purity allows obtaining an improvement in the radiation efficiency, the power balance of the system is analyzed. More in detail, a comparison in terms of reactive power (P_{reac}), radiated power (P_r) and EIRP by using both the BIEs and UIEs is carried out. Indeed, even if the maximum directivity (D) and the modal power excitation are essentially the same as a function of the main beam direction, the modal excitation capability of each source (Fig. 7), as well as the modal excitation purity of each single mode (Table II), are different in case of BIEs and UIEs. This excitation difference should lead a dissimilar power balance of the radiating system. Indeed, the directivity and the percentage power excitation are normalized parameters and not absolute values. Therefore, the power balance is taken into account. In Fig. 13 the comparison between the BIEs and UIEs feeding arrangement is reported as a function of the main beam direction for the evaluation of the reactive power, the radiated power and EIRP. Obviously, the power balance comparison is obtained by considering the same total incident power (1 W). The color plots of Fig. 13*a-d* reveal that the BIEs can minimize the reactive power stored in the near field zone thanks to their better modal excitation purity. Indeed, by using the UIEs, the reactive power of the system (Fig. 13*d*) is considerable higher than the BIEs configuration (Fig. 13*a*). Moreover, from Fig. 13*a* it is visible that, in case of BIEs, higher reactive power are provided when Mode#4 gives a contribution to maximize the directivity (Fig. 11*d*). This is expected since Mode#4 is characterized by the lowest MS and hence it generates greater reactive power when it is stimulated. This behavior is not well visible in case of UIEs (Fig. 13*d*) even if Mode#4 is stimulated in the same areas (Fig. 11*d*). This occurs since a higher number of modes are excited by the UIEs (Fig. 7) and thus the reactive power is very high for every

direction.

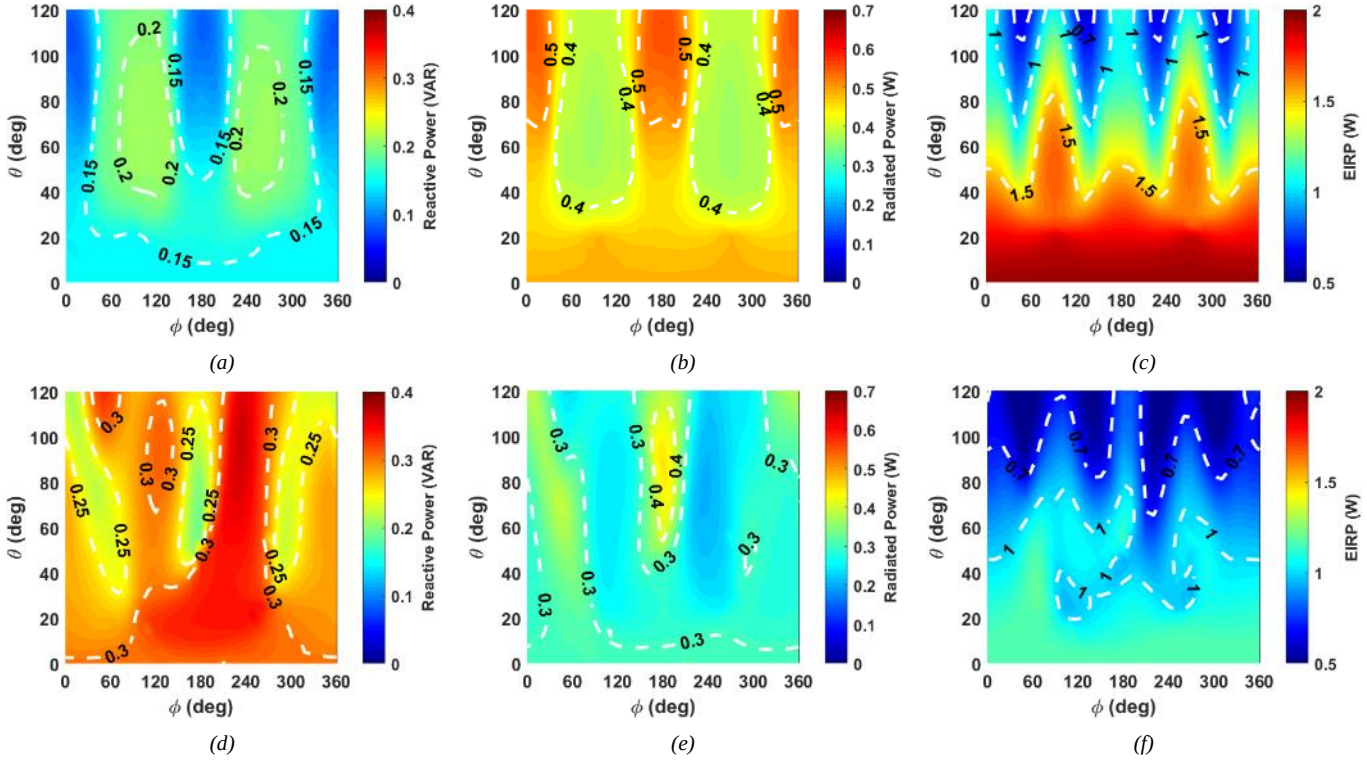

Fig. 13. Power balance comparison between the BIEs and UIEs a function of the main beam direction. *(a)* Reactive Power, *(b)* radiated Power and *(c)* EIRP by resorting to the BIEs; *(d)* reactive power, *(e)* radiated power and *(f)* EIRP by using the UIEs.

It is important to underline that, although some modes do not radiate in far field, they give a significant contribution to the reactive power stored in the near field zone. A lower value of the reactive power plays an important role in the amount of the power delivered to the far field (radiated power). Indeed, as it is well visible through the color maps of Fig. 13*b*- *e*, the radiated power obtained with BIEs presents a significant improvement with respect to UIEs in all the desired main beam directions. Moreover, the behavior of the radiated power is the opposite of the reactive power. More in detail, main beam directions associated to large reactive power correspond to a low radiated power and vice versa.

In addition to the reactive and radiated power, the EIRP of the system has been evaluated by using both the UIEs and BIEs as a function of the main beam direction and the results are shown in Fig. 13*c*-*f*. Obviously, the greater radiated power, as well as almost the same maximum directivity, makes the BIEs a more efficient radiator with a much greater EIRP than the UIEs in all directions.

The different power balance of the system has been also evaluated from a statistical point of view. The C.d.F of the reactive power, radiated power and EIRP have been taken into account with respect to the main beam direction, for both BIEs and UIEs feeding arrangement. More in detail, Fig. 14 and Fig. 15 show the C.d.F of the reactive power and both the radiated power and EIRP, respectively.

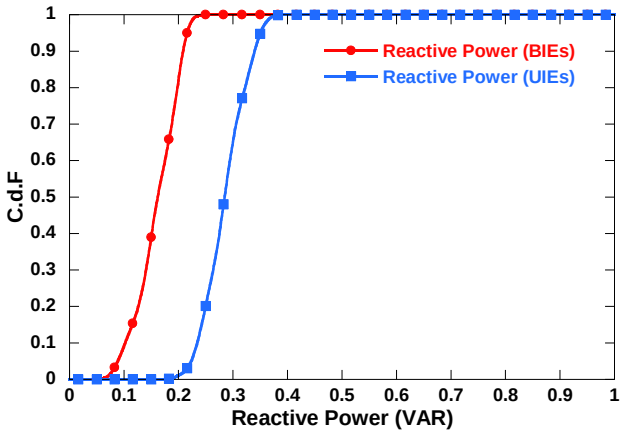

Fig. 14. C.d.F of the reactive power for both BIEs and UIEs feeding arrangement.

In Table III, the mean value of the reactive power and the probability that the $P_{reac} > 0.22$ VAR, are reported. The table underlines the lower mean value (– 43.85%) and the better statistic behaviour of the BIEs with respect the UIEs. The same analysis is also reported in Table IV regarding the mean (μ) of the radiated power and the EIRP. This result emphasizes the more efficient performance of the BIEs also from a statistical point of view. In particular, the better modal excitation purity of the feeding arrangement due to the BIEs allows obtaining an improvement of the mean value of both the radiated power and the EIRP greater than 50 %. For this reason, the BIEs feeding arrangement outperforms the UIEs one from a statistical point

of view as well.

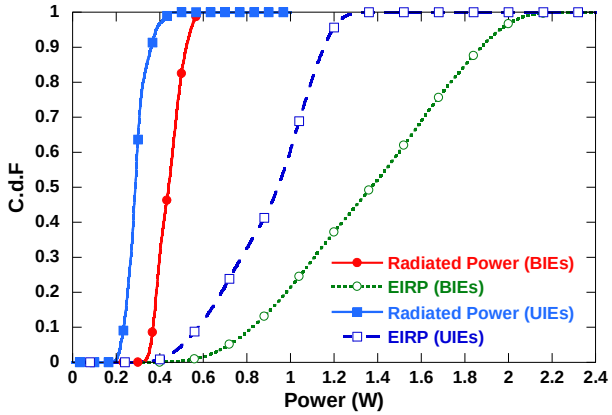

Fig. 15. C.d.F of the radiated power and EIRP for both BIEs and UIEs feeding arrangement.

TABLE III
REACTIVE POWER STATISTICAL COMPARISON

Exciters	Mean of Reactive Power (VAR)	$Pr\,(P_{reac} > 0.22$ VAR)
BIEs	0.160	0.031
UIEs	0.285	0.961
Improvement	– 43.85%	– 96.7%

TABLE IV
RADIATED POWER AND EIRP STATISTICAL COMPARISON

Exciters	P_r		EIRP	
	μ	$Pr\,(P_r > 0.36$ W)	μ	$Pr\,(P_r > 1$ W)
BIEs	0.442	0.94	1.357	0.786
UIEs	0.292	0.1	0.897	0.394
Improvement	51.36%	840%	51.28%	99.4%

V. PROTOTYPES AND MEASUREMENTS

To assess the reliability of the proposed paradigm, four prototypes have been manufactured with an appropriate feeding network to separately excite the first four modes. Moreover, due to the large dimensions of the investigated platform, a scaled version of it (1:30) has been manufactured. The feeding networks used to feed each BIE are shown in Fig. 16. Each feeding network contains Wilkinson Power Dividers (WPDs), delay lines of 180° for each BIE to produce the same flow of current along the loops, and a series capacitors (C) to compensate the inductive behaviors of each small loop and thus obtaining a good impedance matching. As it appears, the first two modes, namely Mode#1 and Mode#2, are stimulated by using two BIEs in phase along the longest and shortest side of the upper rectangular plate, respectively. On the contrary, Mode#3 and Mode#4, are stimulated by using all the four BIEs with an appropriate phase difference as previously reported in Table I. Moreover, in this case the feeding of each BIE is achieved by means of two SMA connectors.

A picture of the fabricated prototype for feeding each BIE is reported in Fig. 17. In particular, the WPD produces two equal signals, the delay line in one branch provides the out-of-phase condition whereas the series capacitor of 0.2 pF guarantees the impedance matching of each loop.

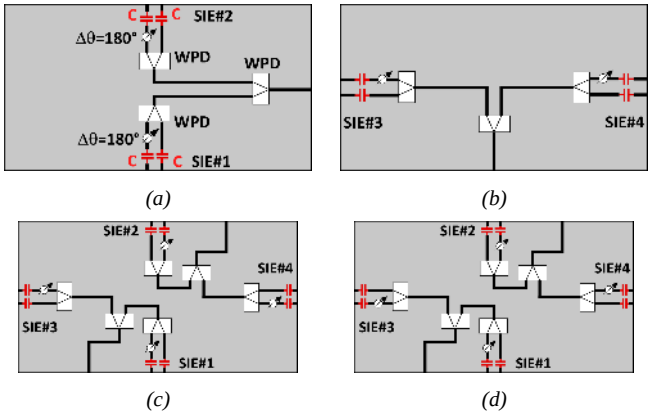

Fig. 16. Feeding network to individually stimulate the desired modes; *(a)* Mode#1, *(b)* Mode#2, *(c)* Mode#3 and *(d)* Mode#4.

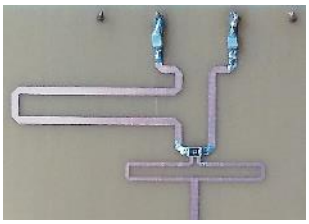

Fig. 17. Required feeding network to feed the BIE.

The feeding network is realized inside the platform with microstrip lines technology by exploiting the upper face of the platform as a ground plane. The total length of each loop has been chosen to provide a real part of the input impedance close to 50 Ω within the frequency range of operation to simplify the matching network between the BIE and the transmission line (only a series capacitor C). More in detail, each half loop presents a length of 8 mm, a height of 4 mm from the upper face of the box, a radius of 0.35 mm whereas the distance between the two half loops is set to 10 mm.

The fabricated prototype with two BIEs and four BIEs are illustrated in Fig. 18. The platform is a handmade wooden box covered with conductive tape. A zoom view of the two loop composing a BIE can be observed in Fig. 18*d*.

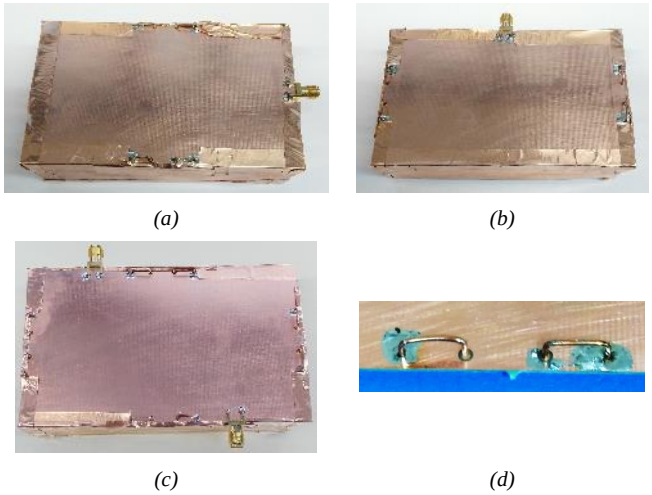

Fig. 18. Fabricated prototype of the rectangular box with the BIEs. *(a)* Two BIEs along the longest side, *(b)* two BIEs along the shortest side and *(c)* four BIEs in the middle of each side and *(d)* zoom of a single BIE.

The comparison between simulated and measured reflection coefficient (S_{11}) on the scaled prototype are reported in Fig. 19. More in detail, Fig. 19*a* shows the S_{11} parameters of the platform with two BIEs along the longest side (Mode#1) and shortest one (Mode#2). On the contrary, the S_{11} parameters regarding the platform with four BIEs (Mode#3 and Mode#4) are shown in Fig. 19*b*. The agreement between simulations and measurements is satisfactory. The small frequency shift between simulations and measurements can be attributed to a not exact height of the loops above the ground plane of the different prototypes with respect the simulations.

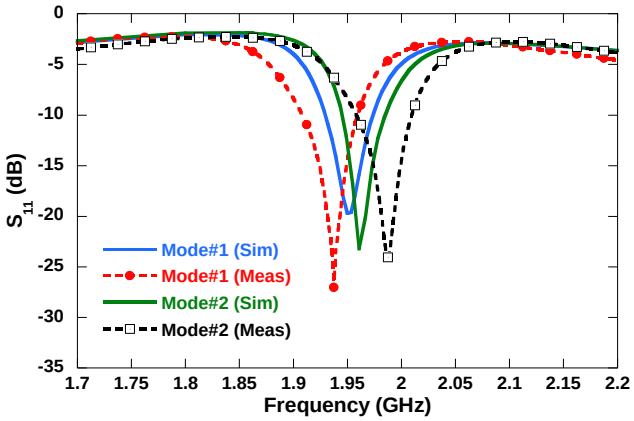

(a)

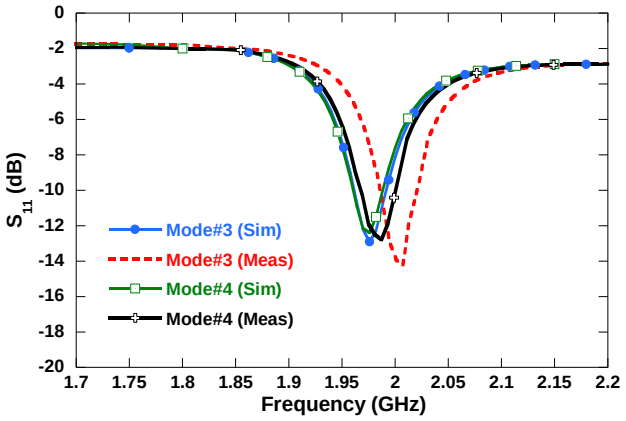

(b)

Fig. 19. Comparison between simulated and measured S_{11} parameter as a function of frequency; *(a)* Mode#1 and Mode#2 Prototype and *(b)* Mode#3 and Mode#4 prototype.

In addition, the normalized radiation patterns of overall platform have been measured when the four modes are individually excited as shown in Fig. 20. It is apparent that simulations and measurements exhibit a good agreement. More in detail, Mode#1 and Mode#2 current modes distributions generate a broadside radiation pattern with orthogonal polarization (Fig. 20*a*-*b*). On the contrary, the radiation pattern associated to Mode#3 and Mode#4 presents a null at broadside direction ($\theta = 0°$).

In addition, the radiation efficiency (η_{rad}) has been taken into account to compare the performance between the BIE and the UIE. In particular, the comparison between the BIE and the UIE in terms of simulated radiation efficiency, by neglecting the feeding network, is reported in Table V when the amplitude and phase difference of Table I are directly applied to the exciters.

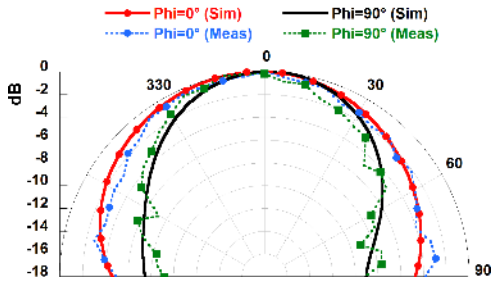

(a)

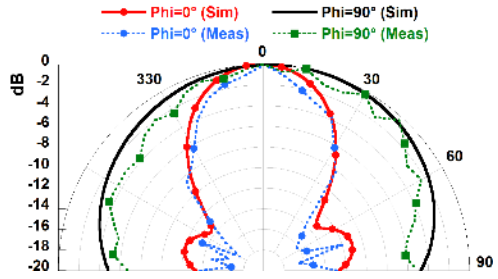

(b)

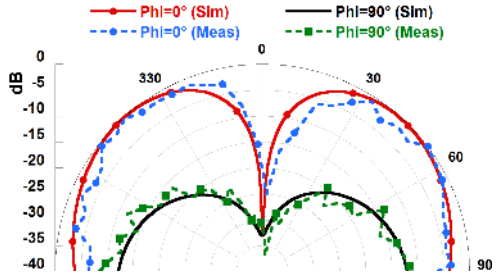

(c)

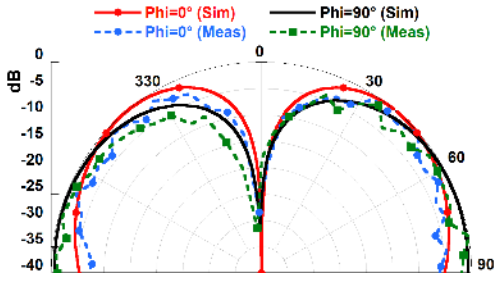

(d)

Fig. 20. Comparison between simulated and measured normalized radiation pattern in the principal planes; *(a)* Mode#1, *(b)* Mode#2, *(c)* Mode#3 and *(d)* Mode#4.

This table emphasizes that the better modal excitation purity obtained by using the novel inductive exciters allows achieving a remarkable improvement of the radiation efficiency, as previously proved in terms of P_r.

Moreover, the η_{rad} has been measured by resorting to the Wheeler cap method [33], [34] for the BIEs case. The comparison, in terms of simulated and measured η_{rad}, is shown in Table VI when the first four modes are stimulated. In this case, the reported values of η_{rad} agrees with the trend of

simulations but are lower than those of Table V due to the losses in the feeding network.

TABLE V
SIMULATED RADIATION EFFICIENCY BY EMPLOYING BOTH THE BIES AND THE UIES FEEDING STRATEGY.

Mode#	BIEs	UIEs
1	0.5	0.32
2	0.49	0.33
3	0.68	0.48
4	0.35	0.23

TABLE VI
COMPARISON BETWEEN THE SIMULATED AND MEASURED RADIATION EFFICIENCY BY EMPLOYING THE BIES FEEDING STRATEGY.

Mode#	Simulated	Measured
1	0.42	0.38
2	0.43	0.36
3	0.52	0.42
4	0.23	0.2

VI. CONCLUSIONS

An innovative design strategy has been proposed for improving the radiation efficiency of a mounted-on-platform radiator by resorting to the CMT. In particular, the use of the CMT has provided helpful information regarding the best exciters positions and feeding to efficiently stimulate current modes (J_n) with the greatest MS on the investigated platform. Furthermore, a novel BIEs able to improve the modal excitation purity has been designed on the basis of the CMT investigation. Moreover, an efficient beam-steering capability has been achieved by means of a multiple CMs excitation operated by the proposed BIEs. A comparison with respect to the UIEs has been performed in terms of P_{reac}, P_r, EIRP, D and percentage power excitation. The results showed that the better modal excitation purity obtained by exploiting the BIEs allows reducing the stored P_{reac} with a consequent significant improvement of the P_r and EIRP. The impact of the dissimilar power balance of the system, due to the both BIEs and UIEs feeding arrangement, has been also evaluated from a statistical point of view. In particular, the BIE enables to achieve an improvement of the mean value of both the radiated power and the EIRP greater than 50 %.

In order to assess the reliability of the proposed BIEs, four prototypes with an appropriate feeding network have been manufactured to excite the first four modes separately. The measured and simulated results present a good agreement and confirm the reliability of the described design process based on the efficient excitation of the CMs by means of the novel BIEs.

REFERENCES

[1] S. Genovesi, A. Monorchio, and S. Saponara, "Compact Triple-Frequency Antenna for Sub-GHz Wireless Communications," *IEEE Antennas Wirel. Propag. Lett.*, vol. 11, pp. 14–17, 2012.

[2] D. Bianchi, S. Genovesi, and A. Monorchio, "Fast Optimization of Ultra-Broadband Antennas With Distributed Matching Networks," *IEEE Antennas Wirel. Propag. Lett.*, vol. 13, pp. 642–645, 2014.

[3] J. V. N. Granger, "Shunt-excited flat-plate antennas with applications to aircraft structures," *Proc. IRE*, vol. 38, no. 3, pp. 280–287, 1950.

[4] R. Tanner, "Shunt and notch-fed HF aircraft antennas," *IRE Trans. Antennas Propag.*, vol. 6, no. 1, pp. 35–43, Jan. 1958.

[5] J. E. Richie and T. J. Barrett, "VHF helicopter antennas that incorporate the airframe and reduce rotor modulation," *IEEE Trans. Electromagn. Compat.*, vol. 42, no. 3, pp. 298–302, 2000.

[6] J. E. Richie and T. Joda, "HF antennas for NVIS applications mounted to helicopters with tandem main rotor blades," *IEEE Trans. Electromagn. Compat.*, vol. 45, no. 2, pp. 444–448, May 2003.

[7] J. E. Richie and B. R. Koch, "The use of side-mounted loop antennas on platforms to obtain nearly omnidirectional radiation," *IEEE Trans. Antennas Propag.*, vol. 53, no. 12, pp. 3915–3919, Dec. 2005.

[8] G. Marrocco and L. Mattioni, "Naval structural antenna systems for broadband HF communications," *IEEE Trans. Antennas Propag.*, vol. 54, no. 4, pp. 1065–1073, Apr. 2006.

[9] G. Marrocco, L. Mattioni, and V. Martorelli, "Naval Structural Antenna Systems for Broadband HF Communications mdash;Part II: Design Methodology for Real Naval Platforms," *IEEE Trans. Antennas Propag.*, vol. 54, no. 11, pp. 3330–3337, Nov. 2006.

[10] L. Mattioni, D. Di Lanzo, and G. Marrocco, "Naval Structural Antenna Systems for Broadband HF Communications—Part III: Experimental Evaluation on Scaled Prototypes," *IEEE Trans. Antennas Propag.*, vol. 56, no. 7, pp. 1882–1887, Jul. 2008.

[11] Y. Chen and C.-F. Wang, *Characteristics modes: theory and applications in antenna engineering*. Hoboken, New Jersey: Wiley, 2015.

[12] H. Li, Y. Tan, B. K. Lau, Z. Ying, and S. He, "Characteristic Mode Based Tradeoff Analysis of Antenna-Chassis Interactions for Multiple Antenna Terminals," *IEEE Trans. Antennas Propag.*, vol. 60, no. 2, pp. 490–502, Feb. 2012.

[13] R. Martens, J. Holopainen, E. Safin, J. Ilvonen, and D. Manteuffel, "Optimal Dual-Antenna Design in a Small Terminal Multiantenna System," *IEEE Antennas Wirel. Propag. Lett.*, vol. 12, pp. 1700–1703, 2013.

[14] K. Kumar Kishor and S. V. Hum, "A Pattern Reconfigurable Chassis-Mode MIMO Antenna," *IEEE Trans. Antennas Propag.*, vol. 62, no. 6, pp. 3290–3298, Jun. 2014.

[15] D. Manteuffel and R. Martens, "Systematic design method of a mobile multiple antenna system using the theory of characteristic modes," *IET Microw. Antennas Propag.*, vol. 8, no. 12, pp. 887–893, Sep. 2014.

[16] C. Deng, Z. Feng, and S. V. Hum, "MIMO Mobile Handset Antenna Merging Characteristic Modes for Increased Bandwidth," *IEEE Trans. Antennas Propag.*, pp. 1–1, 2016.

[17] F. Dicandia, S. Genovesi, and A. Monorchio, "Null-Steering Antenna Design by Using Phase-Shifted Characteristic Modes," *IEEE Trans. Antennas Propag.*, pp. 1–1, 2016.

[18] F. A. Dicandia, S. Genovesi, and A. Monorchio, "Advantageous Exploitation of Characteristic Modes Analysis for the Design of Three Dimensional Null Scanning Antennas," *IEEE Trans. Antennas Propag.*, pp. 1–1, 2017.

[19] D. Manteuffel and R. Martens, "Compact Multimode Multielement Antenna for Indoor UWB Massive MIMO," *IEEE Trans. Antennas Propag.*, vol. 64, no. 7, pp. 2689–2697, Jul. 2016.

[20] A. A. Salih, Z. N. Chen, and K. Mouthaan, "Characteristic Mode Analysis and Metasurface Based Suppression of Higher-Order Modes of a 2 #x00D7;2 Closely-Spaced Phased Array," *IEEE Trans. Antennas Propag.*, vol. PP, no. 99, pp. 1–1, 2017.

[21] F. H. Lin and Z. N. Chen, "Low-Profile Wideband Metasurface Antennas Using Characteristic Mode Analysis," *IEEE Trans. Antennas Propag.*, vol. 65, no. 4, pp. 1706–1713, Apr. 2017.

[22] Y. Chen and C.-F. Wang, "Electrically Small UAV Antenna Design Using Characteristic Modes," *IEEE Trans. Antennas Propag.*, vol. 62, no. 2, pp. 535–545, Feb. 2014.

[23] Y. Chen and C.-F. Wang, "HF Band Shipboard Antenna Design Using Characteristic Modes," *IEEE Trans. Antennas Propag.*, vol. 63, no. 3, pp. 1004–1013, Mar. 2015.

[24] M. Bouezzeddine and W. L. Schroeder, "Design of a Wideband, Tunable 4-port MIMO Antenna System with High Isolation Based on the Theory of Characteristic Modes," *IEEE Trans. Antennas Propag.*, pp. 1–1, 2016.

[25] T.-Y. Shih and N. Behdad, "Bandwidth Enhancement of Platform-Mounted HF Antennas Using the Characteristic Mode Theory," *IEEE Trans. Antennas Propag.*, pp. 1–1, 2016.

[26] R. Martens, E. Safin, and D. Manteuffel, "Inductive and capacitive excitation of the characteristic modes of small terminals," in *Antennas and Propagation Conference (LAPC), 2011 Loughborough*, 2011, pp. 1–4.

[27] R. Martens, E. Safin, and D. Manteuffel, "Selective excitation of characteristic modes on small terminals," in *Antennas and Propagation (EUCAP), Proceedings of the 5th European Conference on*, 2011, pp. 2492–2496.
[28] S. Genovesi, F. A. Dicandia, and A. Monorchio, "Excitation of multiple characteristic modes on a three dimensional platform," in *2017 11th European Conference on Antennas and Propagation (EUCAP)*, 2017, pp. 1769–1771.
[29] R. Harrington and J. Mautz, "Theory of characteristic modes for conducting bodies," *IEEE Trans. Antennas Propag.*, vol. 19, no. 5, pp. 622–628, Settembre 1971.
[30] "FEKO - EM Simulation Software." [Online]. Available: http://www.feko.info.
[31] E. Safin and D. Manteuffel, "Reconstruction of the Characteristic Modes on an Antenna Based on the Radiated Far Field," *IEEE Trans. Antennas Propag.*, vol. 61, no. 6, pp. 2964–2971, Jun. 2013.
[32] "MathWorks - Makers of MATLAB and Simulink." [Online]. Available: http://www.mathworks.com/.
[33] J. González and J. Romeu, "Measurement of radiation efficiency and quality factor of fractal antennas: The wheeler cap method," *FractalComs Inf. Soc. Technol. Programme*, 2002.
[34] H. Choo, R. Rogers, and H. Ling, "On the Wheeler cap measurement of the efficiency of microstrip antennas," *IEEE Trans. Antennas Propag.*, vol. 53, no. 7, pp. 2328–2332, Jul. 2005.